The Effect of Morphological Modification on the Electrochemical Properties of SnO2 Nanomaterials

ARTICLE *in* ADVANCED FUNCTIONAL MATERIALS · FEBRUARY 2008

Impact Factor: 11.81 · DOI: 10.1002/adfm.200700407

5 AUTHORS, INCLUDING:

Min-Sik Park
Korea Electronics Technology Institute
111 PUBLICATIONS **2,532** CITATIONS
SEE PROFILE

Yong-Mook Kang
Dongguk University
111 PUBLICATIONS **2,707** CITATIONS
SEE PROFILE

S. X. Dou
University of Wollongong
1,424 PUBLICATIONS **20,210** CITATIONS
SEE PROFILE

Hua-Kun Liu
University of Wollongong
268 PUBLICATIONS **9,005** CITATIONS
SEE PROFILE

DOI: 10.1002/adfm.200700407

The Effect of Morphological Modification on the Electrochemical Properties of SnO_2 Nanomaterials**

By *Min-Sik Park, Yong-Mook Kang,* Gou-Xiu Wang, Shi-Xue Dou,* and *Hua-Kun Liu**

The electrochemical performances of 1D SnO_2 nanomaterials, nanotubes, nanowires, and nanopowders, are compared to define the most favorable morphology when SnO_2 nanomaterials are adopted as the electrode material for lithium-ion batteries. Changes in the morphology of SnO_2 are closely related with its electrochemical performance. Some SnO_2 nanomaterials feature not only an increased energy density but also enhanced Li^+ transfer. The correlation between the morphological characteristics and the electrochemical properties of SnO_2 nanomaterials is discussed. The interesting electrochemical results obtained here on SnO_2 nanomaterials indicate the possibility of designing and fabricating attractive nanostructured materials for lithium-ion batteries.

1. Introduction

One-dimensional (1D) nanomaterials have attracted a great deal of interest because of their various possibilities in nanoscience and nanotechnology.[1–4] Significant progress has been reported in the use of nanomaterials as electrode materials for lithium-ion batteries. In practice, their large surface-to-volume ratio and relatively short diffusion length could enhance the electrochemical as well as kinetic properties.[5–8] Because of their controlled shape and size on the nanometer scale, these nanomaterials may help in the development of the next generation of advanced lithium-ion batteries. An interesting aspect of the development in lithium-ion batteries is the drive to design and manufacture new anode materials with stable cyclic retention and higher reversible capacity for Li^+ compared to the commercial anode material, graphite (372 mAh g^{-1}).[9–11] Because SnO_2-based materials have already been suggested as the most promising candidates for anode materials in terms of their theoretical reversible capacity (790 mAh g^{-1}), structural modifications of SnO_2 have been attempted to make its electrochemical performance sufficient for commercialization.[12–14] However, the undesirable Li_2O phase formation and volume expansion of the Sn phase constitute the main barriers that have to be overcome. The oxidation reactions in Equations 1 and 2 below describe not only Li_2O formation, but also the volume expansion of Sn:[15]

$$SnO_2 + 4Li^+ + 4e^- \rightarrow 2Li_2O + Sn \quad \text{(large irreversible capacity)} \tag{1}$$

$$Sn + xLi^+ + xe^- \rightarrow Li_xSn (0 \leq x \leq 4.4) \quad \text{(large volume variation)} \tag{2}$$

It is well documented that the Li_2O phase is electrochemically inactive and non-conductive, which is the main reason for the large initial irreversible capacity and the large volume variation of the Sn phase, leading to an abrupt capacity fading during cycling. However, the Li_2O phase could be decomposed, and the volume expansion of the Sn phase could be effectively reduced if the material were in the nanoscale form, according to some earlier reports.[16–19] These reports have attracted significant attention to structural modifications of SnO_2 on the nanoscale, because the electrochemical performance of SnO_2 seems to have a strong correlation to the structural features of the SnO_2 phase. Such modifications might then allow us to reduce the initial irreversible capacity and improve the cyclic retention in the SnO_2 nanomaterials. So far, there is practically no information on the correlation between electrochemical properties and the different crystallographic structures of SnO_2 nanomaterials. However, there is reason to expect that structural modification could be a general solution to the problem of large initial irreversible capacity and poor cyclic retention of SnO_2-based anode materials. Herein, we introduce distinctive electrochemical performances in different types of SnO_2 nanomaterials, such as nanotubes, nanowires, and nanopowders. The relationships between

[*] Dr. Y. M. Kang
Energy Lab, Samsung SDI Co., LTD
428-5, Gongse-ri, Giheung-eup, Yongin-si, Gyeonggi-do (Korea)
E-mail: dake@kaist.ac.kr

Prof. H. K. Liu, M. S. Park, Prof. S. X. Dou
Institute for Superconducting and Electronic Materials and
ARC Centre of Excellence for Electromaterials Science
University of Wollongong
Wollongong NSW 252 (Australia)
E-mail: hua@uow.edu.au

Dr. G.X. Wang
School of Mechanical, Materials and Mechatronic Engineering
University of Wollongong
Wollongong NSW 2522 (Australia)

[**] Financial support provided by the Australian Research Council through the ARC Centre of Excellence (CE0561616) and ARC Discovery (DP0559891) projects is gratefully acknowledged. The authors thank Dr. T. Silver at the University of Wollongong (Australia) and Dr. H. S. Kim at the University of Pennsylvania (USA) for their contributions. Supporting Information is available online from Wiley InterScience or from the authors.

different structural features such as surface area, porosity, and electronic conductivity from different crystallographic structures and observed electrochemical properties are discussed to determine the advantages of 1D nanomaterials. Furthermore, the promising possibilities of 1D SnO_2 nanomaterials are emphasized from the electrochemical point of view.

2. Results and Discussion

2.1. Material Preparation and Characterization

For the purpose of demonstrating the effect of morphological modification on the electrochemical performance of SnO_2, three different types of SnO_2 nanomaterials (nanotubes, nanowires, and nanopowders) were synthesized for use as anode materials. Typical field-emission scanning electron microscopy (FESEM) images of SnO_2 nanomaterials at different magnifications are displayed in Figure 1. The SnO_2 nanotubes prepared by a sol–gel templating route combined with a vacuum-suction method possess a tubular structure with open tips. They have a uniform outer diameter of around 200 nm and well-defined inner holes as shown in Figure 1a and b. It was expected that the tubular structure of SnO_2 nanotubes would be providing more reaction sites, with the additional advantage that their porous wall structure could accommodate a volume variation of the Sn phase during cycling. In the case of SnO_2 nanowires synthesized by thermal evaporation, SEM observations clearly show randomly aligned SnO_2 nanowires with diameters of 100–300 nm and lengths extending to several tens of micrometers (Fig. 1c and d). It has been well documented that single-crystalline nanowires have some advantages for electronic conduction and Li^+ diffusion, which leads to the improvement of kinetic properties. In comparison, SnO_2 nanopowders prepared by a conventional sol–gel method have a particle size of less than 100 nm on average and a clean surface without obvious irregular ravines (Fig. 1e and f). The particle agglomeration observed in SnO_2 nanopowders results from local van der Waals forces.

In order to determine the structural features of these nanomaterials with different morphological characteristics, their phase and crystallinity were confirmed by X-ray diffraction (XRD) and Raman spectroscopy. As shown in Figure 2, all reflections of SnO_2 nanomaterials were in excellent accordance with a tetragonal rutile structure (JCPDS 41-1445), which belongs to the space group $P4_2/mnm$ (136). There was no notable peak shifting or intensity variation induced by secondary phases or impurities. Within the margins of errors, the lattice parameters, volume, lattice strain, and density of the nanomaterials could be estimated by using Rietveld refinement as summarized in Table 1. Because the reference SnO_2 phase has lattice parameters of $a = b = 4.7386$ Å and $c = 3.1872$ Å, it can be said that for our nanomaterials, there is no significant difference related to substitutional or interstitial occupancy of impurities compared to the reference material. We only found a small extension of the *c*-axis lattice parameter of the nanowires and nanotubes, which might be caused by more tensile stress along the *c*-axis, and a small reduction of the *c*-axis for the nanopowders because of their small dimensions.[5] With regard to the behavior of the full width at half maximum (FWHM) values, the SnO_2 nanotubes show an apparently larger peak broadening compared to the other nanomaterials. So far as strain is concerned, the

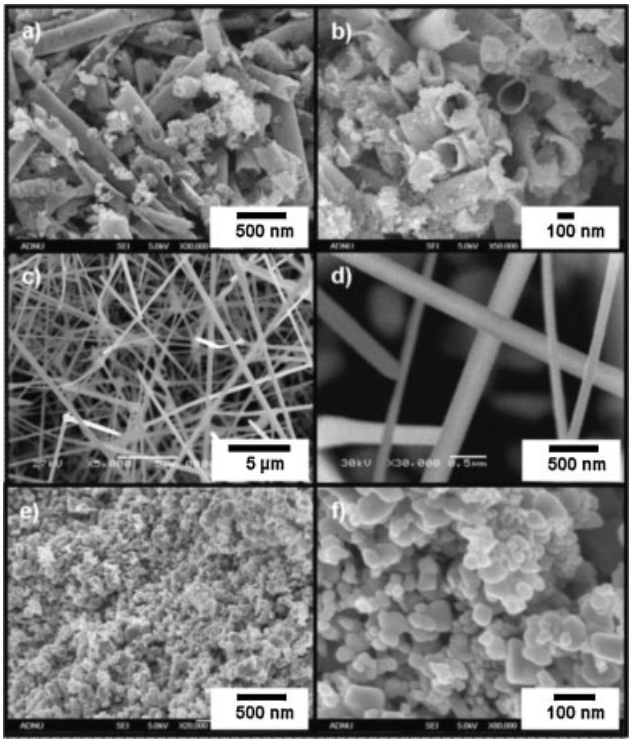

Figure 1. The microstructures of SnO_2 nanomaterials: a,b) FESEM images of SnO_2 nanotubes; c,d) FESEM images of SnO_2 nanowires; e,f) FESEM images of SnO_2 nanopowders at different magnifications.

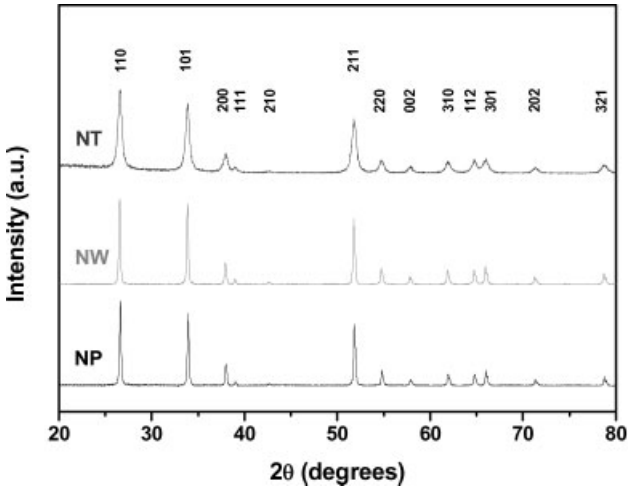

Figure 2. X-ray diffraction patterns of SnO_2 nanomaterials: nanotubes (NT), nanowires (NW), and nanopowders (NP).

ADVANCED FUNCTIONAL MATERIALS

Table 1. Rietveld refinement results for SnO_2 nanomaterials.

	a [Å]	c [Å]	Volume [Å^3]	Strain [%]	Density [g · cm^{-3}]
NT[a]	4.7384(3)	3.1874(7)	71.62	0.497(7)	7.0358
NW[b]	4.7386(2)	3.1882(1)	71.57	0.117(5)	7.1309
NP[c]	4.7372(5)	3.1864(2)	71.53	0.113(2)	6.9985

[a] SnO_2 nanotubes. [b] SnO_2 nanowires. [c] SnO_2 nanopowders.

Table 2. Surface areas and electrical conductivities of SnO_2 nanomaterials.

	Conductivity σ [S · cm^{-1}]	Surface area [m^2 · g^{-1}]	Pore volume [cm^3 · g^{-1}]
NT[a]	6.023×10^{-8}	231.28	0.84
NW[b]	2.531×10^{-7}	146.56	0.25
NP[c]	1.242×10^{-8}	97.32	0.38

[a] SnO_2 nanotubes. [b] SnO_2 nanowires. [c] SnO_2 nanopowders.

lattice strain is directly caused by variations in the *d*-spacing, if there is no uniform stress over a long distance induced by dislocations or lattice distortions. The nanotubes show much larger strain values compared to that of the nanopowders in Table 1. The larger strain induced by the internal stress from maintaining its unique nanostructure and from the nanopores in the walls could lead to peak broadening. In addition, a small value of the coherence area, which results in broadening of the reflections in the XRD patterns, is found for the polycrystalline nanotubes, which is unlike the pattern for single-crystalline nanowires. This is thought to be characteristic of the fine tubular structure.[8,16] In the case of nanowires, there were small reductions in the FWHM values compared to the nanopowders, corresponding to grain growth or enlargement of the crystal size.

Figure 3 shows room-temperature Raman spectra of the SnO_2 nanomaterials. The fundamental Raman scattering peaks for the SnO_2 nanopowders were observed at 477 cm^{-1}, 636 cm^{-1}, and 777 cm^{-1}, corresponding to the E_g, A_{1g}, and B_{2g} vibration modes, respectively.[20] We also found these peaks in the Raman spectra of the nanotubes and nanowires. As shown in Figure 3, the downwards shift of the B_{2g} vibration mode in SnO_2 nanotubes (776 cm^{-1}) and nanowires (775 cm^{-1}) could be caused by the size effect of the structure.[21] It is well known that the spectra are highly dependent on excitations from the resonance behavior. They could also be influenced by structural factors or the wavelength of laser. Inspection of these spectra indicates that the resonance might be influenced by the different nanostructures in our samples.[21]

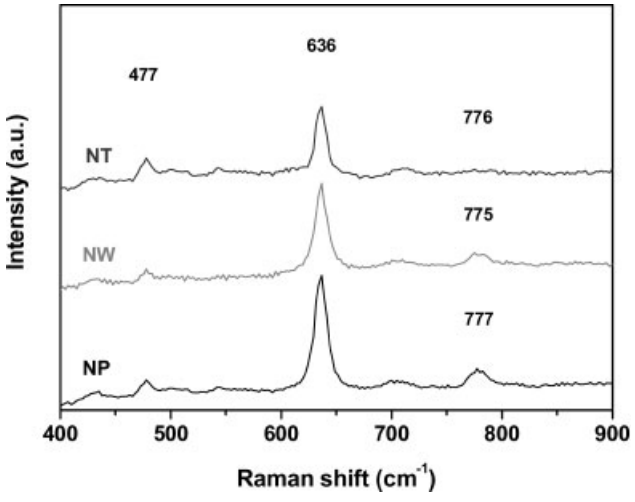

Figure 3. Room-temperature Raman spectra of SnO_2 nanomaterials: nanotubes (NT), nanowires (NW), and nanopowders (NP).

The typical specific surface areas and pore volumes of the SnO_2 nanomaterials were estimated by Brunauer–Emmett–Teller (BET) and Barrett–Joyner–Halenda (BJH) analyses, respectively (Table 2). The variations in the surface area and pore volume were highly dependent on the morphological features, as shown in the FESEM images. The porous polycrystalline nanotubes and the single-crystalline nanowires have larger surface areas than the nanopowders. This means that the nanotubes and nanowires with their high aspect ratios (length/diameter) could provide more reaction sites for Li^+ than the nanopowders. In addition, a comparison of the electrical conductivity for the SnO_2 nanomaterials convinced us that there is a correlation between the morphological characteristics and Li^+ transfer. Even though the mechanism of Li^+ transfer in the solid state is not clear, it is believed that nanowires show a better Li^+ transfer efficiency compared to the other nanomaterials. Note that the nanowires show a relatively higher conductivity (Table 2).

Transmission electron microscopy (TEM) observations confirmed the microstructure of our SnO_2 nanomaterials. The nanotubes have a porous wall structure composed of ultrafine nanopowders with sizes of less than 100 nm, as shown in Figure 4a. There seems to be an agglomeration of nanopowders with high aspect ratio along the length direction and hollow inner holes, including fine nanopores on the wall. The corresponding ring-like selected-area electron diffraction (SAED) pattern indicates that the nanotubes have a polycrystalline structure, and the diffraction rings from inside to outside can be indexed to the (110), (101), (200), (211), (301), and (002) planes of rutile SnO_2, respectively. These indexed patterns are in good accordance with the XRD reflections above. Comparing the SAED patterns of the nanotubes with those of the nanopowders, only blurred patterns and small spots could be derived from the porous structure of the nanotubes. On the other hand, TEM images of the SnO_2 nanowires reveal a fine microstructure, each wire being a single crystal with a tetragonal structure (Figure 4b). Tilting experiments also revealed no evidence of extended defects within the individual crystals. From the TEM image and SAED patterns, we found that the zone axis is [001], and the growth direction of the nanowire is parallel to [100]. In accordance with our previous observations, we also confirmed that the

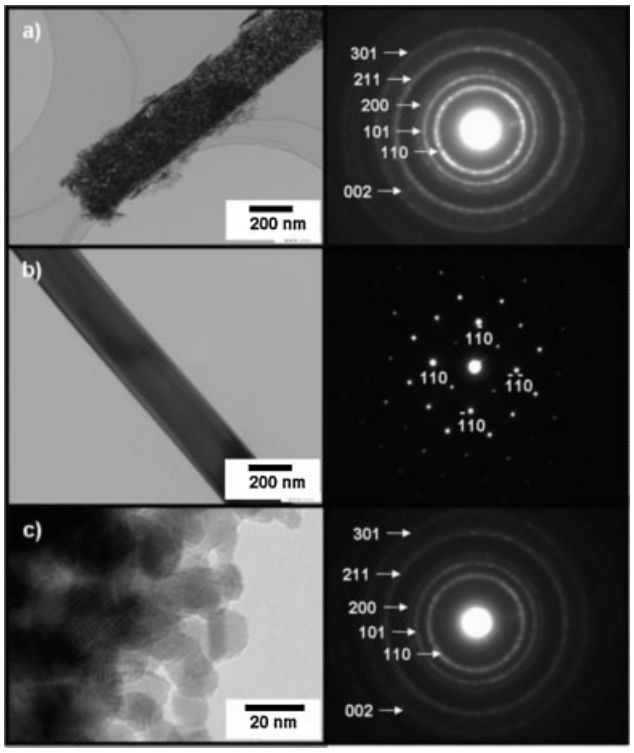

Figure 4. TEM observations and selected-area diffraction (SAED) patterns of a) SnO_2 nanotubes, b) SnO_2 nanowires [5], and c) SnO_2 nanopowders.

nanopowders exist in the form of agglomerated nanoparticles with a size of less than 30 nm, as shown in Figure 4c.

2.2. Electrochemical Properties

The electrochemical reactivity of the SnO_2 nanomaterials over the potential range of 0.05 V to 1.50 V was tested up to fifty cycles. There are apparent differences in the electrochemical behavior of the different morphological structures. From the galvanostatic voltage profiles for the first cycle, we found that the nanowires and nanotubes show improved initial coulombic efficiencies compared to the nanopowders, as illustrated in Figure 5a. The first discharge capacities of the nanowires (2137 mAh g^{-1}), the nanotubes (2304 mAh g^{-1}), and the nanopowders (1850 mAh g^{-1}) are in proportion to the surface area, whereas the initial irreversible capacities of the nanowires (1134 mAh g^{-1}), the nanotubes (1384 mAh g^{-1}), and the nanopowders (1277 mAh g^{-1}) are in proportion to the pore volume. It should be noted that the SnO_2 nanowires and nanotubes show initial coulombic efficiencies of approximately 46.91% and 39.31%, respectively, which are notably higher than that of the SnO_2 nanopowders, 31.01%. The electrochemical dependence of the SnO_2 nanomaterials on their morphological characteristics could be explained by the enhanced electronic conduction and charge transfer of SnO_2 nanowires and nanotubes along the length direction. This is because the SnO_2 nanowires and nanotubes feature a high

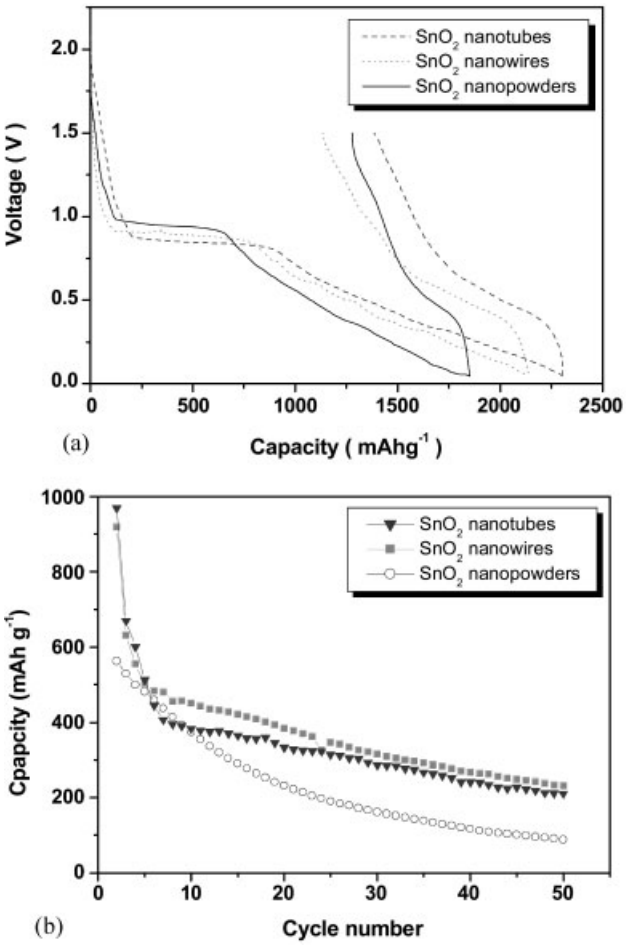

Figure 5. The anodic performances of the SnO_2 nanomaterials: a) the galvanostatic voltage profiles between 0.05 V and 1.50 V for the first cycle, b) the cyclic performance of SnO_2 nanomaterials up to the fiftieth cycle at the same current density, 100 mA g^{-1}.

aspect ratio, which may provide better Li^+ transfer and more reaction sites.

From Table 2 it can be seen that the resistance of the nanowires and nanotubes is much lower than that of nanopowders. This phenomenon implies that the reversible movement of Li^+ into SnO_2 nanowires or nanotubes is much less restrained than that into SnO_2 nanopowders. Actually, the initial Li^+ insertion into nanopowders induced a more drastic potential drop compared to the insertion into nanowires and nanotubes, as shown in Figure 5a. Because the initial ion insertion is accompanied by activation polarization linked to the electronic conductivity of the electrode materials, this result may prove that the electrochemical performance of SnO_2 greatly depends on it electronic conductivity.[22] This kinetic advantage of nanowires and nanotubes also induced a more stable cyclic retention compared to that of nanopowders. In Figure 5b, the SnO_2 nanowire and nanotube electrodes exhibited a higher reversible specific capacity of over 300 mAh g^{-1} up to the fiftieth cycle with relatively stable cyclic performance, whereas the nanopowder electrode

showed an abrupt capacity fading. The average capacity fading of the nanowires and nanotubes was estimated to be 1.45% and 1.87% per cycle after the second cycle, which was much smaller than that of the SnO_2 nanopowders, 3.46%. Based on these results and this discussion, it could be concluded that suitable morphological modification can lead to strong enhancement of the electrochemical performance of electrode materials. When the cyclic retentions of nanomaterials are compared, it seems likely that undesirable Li^+ trapping or loss of electronic connection between active materials caused by volume variation could be most effectively prevented in the single-crystalline nanowire form. The very small disparity between the cyclic retention of nanowires and nanotubes implies that the electrochemical improvement in nanowires and nanotubes should be mainly attributed to their 1D microstructure.

To identify the electrochemical reactions during cycling, cyclic voltammetry (CV) measurements were performed on the SnO_2 nanowires and nanotubes and the results are presented in Figure 6. The CV profiles for the nanowires show two apparent reduction peaks around 0.95 V and 1.20 V, which can be derived from Li_2O formation and electrolyte decomposition when the SnO_2 nanowires react with Li^+ as described in Equation 1. These peaks are leaving a large initial irreversible capacity in the first cycle of SnO_2 nanowire electrodes. The other pairs of reduction and oxidation peaks at 0.25 V and 0.60 V during discharging and at 0.50 V and 0.70 V during charging are related to the formation of Li_xSn as described in Equation 2. Even though there is peak broadening in the CV of the nanowires, we found the same peaks in the CV profiles for the SnO_2 nanotubes over the same potential range. Thus, it was confirmed that the morphological modification of materials does not have an effect on the kind of redox reactions. Electrochemical impedance spectroscopy (EIS) was conducted to determine the Li^+ transfer behavior in SnO_2 nanotubes and nanowires. It is well known that the high-frequency semicircle can be attributed to the contact resistance occurring because of the solid-electrolyte-interphase (SEI) film, the medium-frequency semicircle is related to the charge-

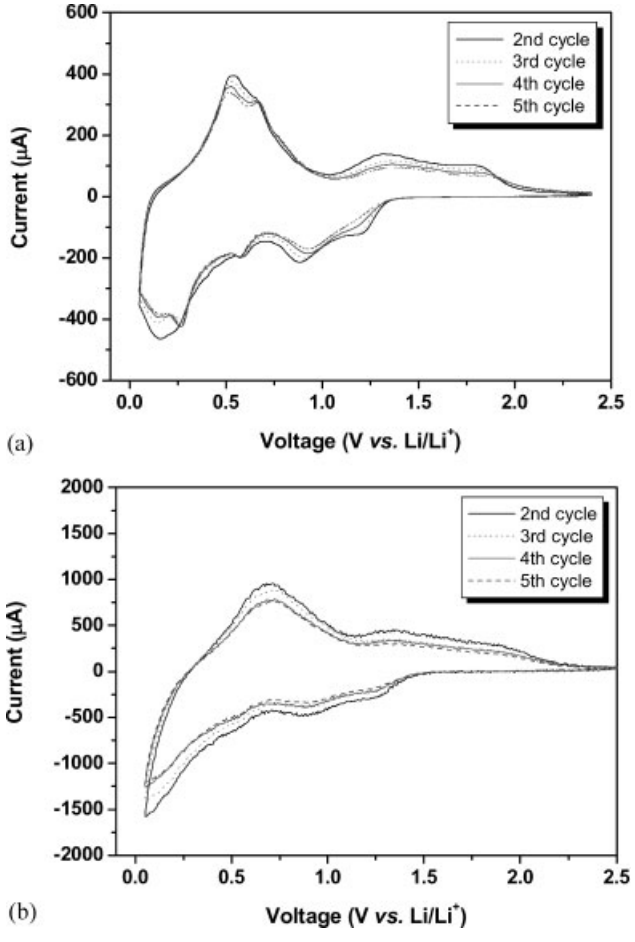

Figure 6. Cyclic voltammetry (CV) profiles of SnO_2 nanomaterials: a) CV curves of SnO_2 nanotubes and b) CV curves of SnO_2 nanowires from the second cycle to the fifth cycle.

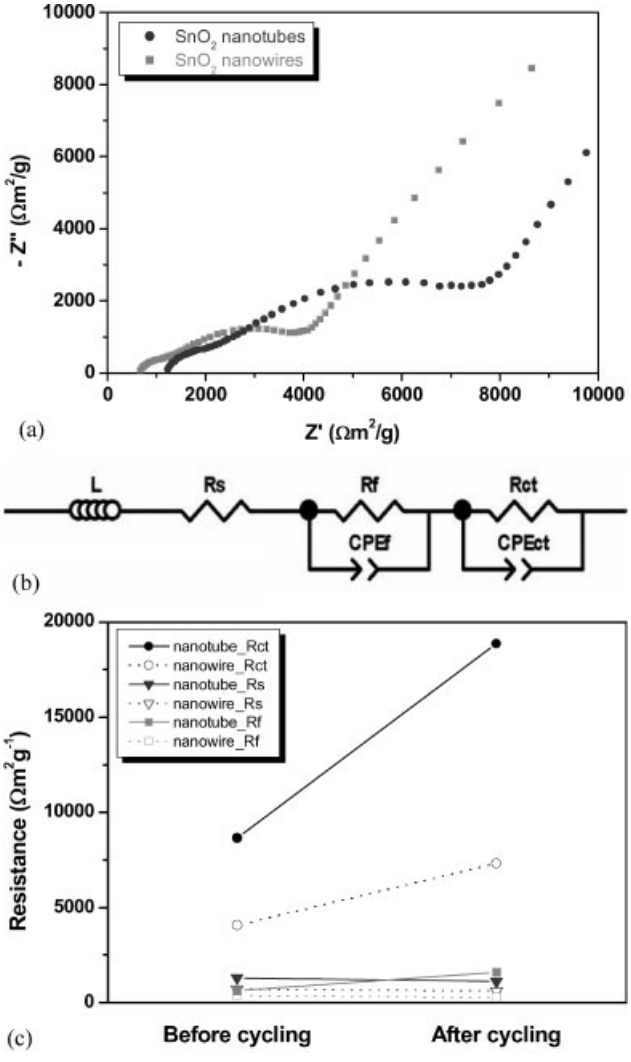

Figure 7. Impedance spectra of SnO_2 nanotubes and SnO_2 nanowires measured at the open circuit potential of 2.0 V: a) Nyquist plots with normalized impedance before cycling, b) the equivalent circuit that was used to fit the impedance data, c) the variation of intrinsic resistances (R_s, R_f, R_{ct}).

transfer resistance at the interface between the electrolyte and the electrode material, and the inclined lines correspond to the Li^+ diffusion process inside the electrode material.[23] From a pure electrical point of view, the experimental data could be satisfactorily fitted using an equivalent circuit with only slight differences in the goodness of the fit. As observed in carbonaceous material, Li^+ insertion tends to diminish the impedance. Because the alloying between Li^+ and Sn involves the augmentation of surface area, which is in inverse proportion to the impedance, Li^+ insertion into SnO_2 could make the reduction in impedance more prominent.[23–25] Figure 7c shows the variation of the intrinsic resistances (R_s, R_f, and R_{ct}). From Figure 7a, it can be observed that the nanotubes have a larger contact resistance (R_f) in the high-frequency region, while the charge-transfer resistance (R_{ct}) in the medium-frequency range is also larger for nanotubes than for nanowires. This may be related to the disparity between the nanotubes and nanowires in their surface area and electronic conductivity. Considering that the faradaic reaction is determined by ion transfer and electron conduction, the better electronic conductivity of the nanowires may play the crucial role in the reduction of the resistance. After cycling (5 cycles), the nanowire electrode still shows a smaller resistance compared to the nanotube electrode, as indicated in Figure 7c. Therefore, it should be noted that charge transfer is highly dependent on the morphological features of the electrode material.

3. Conclusions

The experiments described here clearly demonstrate that the electrochemical performance of SnO_2 nanomaterials is likely to be related to their morphological features. The specific surface areas are mainly attributable to Li^+ storage, and single-crystalline structures are better for maintaining electronic conductivity and allowing enhancement of Li^+ diffusion into the SnO_2 structure. Despite the fact that porous structures are generally more suitable for accommodating volume variations of the Sn phase during cycling, they may also trap more Li^+ during electrochemical cycling, resulting in large irreversible capacities. The use of SnO_2 nanomaterials gives an important indication for the further improvement of the electrochemical properties of SnO_2 systems.

4. Experimental

Preparation of SnO_2 Nanopowders: Nanocrystalline SnO_2 nanopowders were synthesized by a conventional sol–gel method as follows: 3 M of Sn^{II} solution was prepared by dissolving 0.338 g of $SnCl_2 \cdot 2H_2O$ (99.99%, Aldrich) in a mixture of ethanol (0.47 mL) and 36% HCl (0.03 mL). The solution was aged for 24 hours, and then water (0.03 mL) was added under continuous stirring for 12 h. After the formation of the gel, it was dried at 120 °C for 2 hours and sintered at 600 °C for 3 h in a vacuum furnace under an Ar (95%) and O_2 (5%) atmosphere. To remove Cl^-, the final product was washed with distilled water via a centrifugal process and dried at 120 °C for 2 h in a vacuum oven.

Preparation of SnO_2 Nanotubes: SnO_2 nanotubes were prepared via a sol–gel vacuum-suction method. 10 mL of a 3 M Sn^{II} solution was prepared as outlined above. The Sn-based solution was inserted into the nanoholes of anodic aluminum oxide (AAO) templates by a reduced vacuum-suction process. The product was dried at 120 °C for 2 h and sintered at 400 °C for 3 h in a vacuum furnace under an Ar (95%) and O_2 (5%) atmosphere. The AAO templates were dissolved in a 6 M NaOH solution. Then, the product was washed with distilled water by centrifuging and finally dried in a vacuum oven.

Preparation of SnO_2 Nanowires: A thermal-evaporation process was employed to synthesize the SnO_2 nanowires. For the evaporation source, high-purity SnO (99.99%, Aldrich) and Sn (99.99%, Aldrich) powders were homogeneously mixed in a 1:1 weight ratio by planetary mechanical milling for 40 h under an Ar atmosphere. An alumina boat containing 1 g of ball-milled powder was placed inside a tube furnace. Silicon substrates without metal catalysts were placed downstream one by one at a distance of about 15 cm from the powder. The processing temperature and time were optimized at 900 °C and 1 h, respectively. The deposition pressure was around 100 Torr of high-purity Ar gas at a flow rate of 50 sccm (standard cubic centimeters per minute). [5]

Electrochemical Experiments: To make electrodes, a mixture of 75 wt % of each active material and 15 wt % acetylene black was added to a solution containing 10 wt % polyvinylidene fluoride (PVDF) in *n*-methyl-2-pyrrolidinone (NMP). This slurry was pasted onto a copper foil current collector and dried at 110 °C for 2 h in vacuum (10^{-3} Torr). After pressing under a pressure of about 200 kg cm^{-2}, half cells (CR2032 coin-type) were fabricated to evaluate the anodic performance of the SnO_2 nanomaterials. The assembly was carried out in an Ar-filled glove box with less than 0.1 ppm each of oxygen and moisture. A Li metal foil was used as the counter and reference electrode, and 1 M of $LiPF_6$ dissolved in a 1:1 (v/v, Merck KGaA) mixture of ethylene carbonate (EC) and dimethyl carbonate (DMC) was employed as the electrolyte. Charge–discharge tests and CV tests on the SnO_2 nanomaterials were performed up to the fiftieth cycle in the range of 0.05 to 1.5 V (vs. Li/Li^+).

Structural and Morphological Characterization: The microstructure and morphology of SnO_2 nanomaterials were characterized by X-ray diffraction (Philips 1730), Raman spectroscopy (Jobin Yvon HR800), field-emission scanning electron microscopy (JEOL JEM-3000), and transmission electron microscopy (JEOL 2011). In order to measure the conductivity of the SnO_2 nanomaterials, a Jandel four-point probe technique was adopted. Finally, the pore volume and surface area of our SnO_2 nanomaterials were estimated by Barret–Joiner–Halenda (BJH) and Brunauer–Emmett–Teller (BET) analyses, respectively.

Received: April 10, 2007
Revised: September 20, 2007

[1] Y. Cui, Q. Q. Wei, H. K. Park, C. M. Lieber, *Science* **2001**, *293*, 1289.
[2] Y. Huang, X. Duan, Y. Cui, L. J. Lauhon, K. H. Kim, C. M. Lieber, *Science* **2001**, *294*, 1313.
[3] P. G. Collins, M. S. Arnold, P. Avouris, *Science* **2001**, *292*, 706.
[4] A. Bachtold, P. Hadley, T. Nakanishi, C. Dekker, *Science* **2001**, *294*, 1317.
[5] M. S. Park, G. X. Wang, Y. M. Kang, D. Wexler, S. X. Dou, H. K. Liu, *Angew. Chem. Int. Ed.* **2007**, *46*, 750.
[6] Y. Wang, H. C. Zeng, J. Y. Lee, *Adv. Mater.* **2006**, *18*, 645.
[7] X. W. Lou, Y. Wang, C. Yuan, J. Y. Lee, L. A. Archer, *Adv. Mater.* **2006**, *18*, 2325.
[8] Y. Wang, K. Takahashi, K. Lee, G. Cao, *Adv. Funct. Mater.* **2006**, *16*, 1133.
[9] J. M. Tarascon, M. Armand, *Nature* **2001**, *414*, 359.
[10] J. R. Dhan, T. Zheng, Y. Liu, J. S. Xue, *Science* **1995**, *270*, 590.

ADVANCED FUNCTIONAL MATERIALS

[11] M. Winter, J. O. Besenhard, M. E. Spahr, P. Novak, *Adv. Mater.* **1998**, *10*, 725.
[12] Y. Idota, T. Kubota, A. Matsufuji, Y. Maekawa, T. Miyasaka, *Science* **1997**, *276*, 1395.
[13] I. A. Courtney, J. R. Dahn, *J. Electrochem. Soc.* **1997**, *144*, 2045.
[14] J. O. Besenhard, J. Yang, M. Winter, *J. Power Sources* **1997**, *68*, 87.
[15] N. Li, C. R. Martin, B. Scrosati, *Electrochem. Solid State Lett.* **2000**, *3*, 316.
[16] S. A. Needham, G. X. Wang, H. K. Liu, *J. Power Sources* **2006**, *159*, 254.
[17] P. Pizot, S. Laruelle, S. Grugeon, L. Dupont, J. M. Tarascon, *Nature* **2000**, *407*, 496.
[18] M. N. Obrovac, R. A. Dunlap, R. J. Snaderson, J. R. Dahn, *J. Electrochem. Soc.* **2001**, *148*, A576.
[19] H. Li, X. Huang, L. Chen, Z. Wu, Y. Liang, *Electrochem. Solid State Lett.* **1999**, *2*, 547.
[20] J. Fan, T. Wang, C. Yu, B. Tu, Z. Jiang, D. Zhao, *Adv. Mater.* **2004**, *16*, 1432.
[21] I. H. Campbell, P. M. Fauchet, *Solid State Commun.* **1986**, *58*, 739.
[22] Y. M. Kang, S. M. Lee, S. J. Kim, G. J. Jeong, M. S. Sung, W. U. Choi, S. S. Kim, *Electrochem. Commun.* **2007**, *9*, 959.
[23] S. Yang, H. Song, X. Chen, *Electrochem. Commun.* **2006**, *8*, 137.
[24] Y. M. Kang, J. Y. Go, S. M. Lee, W. U. Choi, *Electrochem. Commun.* **2007**, *9*, 1276.
[25] Y. M. Kang, M. S. Park, M. S. Song, J. Y. Lee, *J. Power Sources* **2006**, *162*, 1336.

